JGR Solid Earth

RESEARCH ARTICLE
10.1029/2023JB027991

The Architecture of a Root Zone of a Large Magmatic Conduit System From High Resolution Magnetic, Gravity and Petrophysical Data: The Reinfjord Ultramafic Complex

Z. Pastore[1], N. S. Church[1], C. Fichler[1], A. Michels[1,2], G. W. ter Maat[1,3], R. B. Larsen[1], and S. A. McEnroe[1]

[1]Department of Geoscience and Petroleum, Norwegian University of Science and Technology, Trondheim, Norway, [2]Now at Department of Physics & Astronomy, Howard University, Washington, DC, USA, [3]Now at Utrecht University, Utrecht, The Netherlands

Key Points:

- The modeled structure of the ultramafic complex resulted in a minimum volume of 6.5 km^3 and an eastward plunging root with depth of 1.4 km
- Modeling results suggest localized serpentinization of ultramafic rocks with shallow to negative natural remanent magnetization (NRM) inclination and high Königsberger ratio
- A new proposed uplift history for the Seiland Igneous Province indicating the southern part as a deeper section of the continental crust

Supporting Information:

Supporting Information may be found in the online version of this article.

Correspondence to:

Z. Pastore,
zeudia.pastore@ntnu.no

Citation:

Pastore, Z., Church, N. S., Fichler, C., Michels, A., ter Maat, G. W., Larsen, R. B., & McEnroe, S. A. (2024). The architecture of a root zone of a large magmatic conduit system from high resolution magnetic, gravity and petrophysical data: The Reinfjord ULTRAMAFIC complex. *Journal of Geophysical Research: Solid Earth*, *129*, e2023JB027991. https://doi.org/10.1029/2023JB027991

Received 2 OCT 2023
Accepted 28 MAR 2024

Author Contributions:

Conceptualization: Z. Pastore, N. S. Church, C. Fichler, S. A. McEnroe
Data curation: Z. Pastore, N. S. Church, A. Michels, G. W. ter Maat
Formal analysis: Z. Pastore, N. S. Church, A. Michels, G. W. ter Maat, R. B. Larsen
Funding acquisition: R. B. Larsen, S. A. McEnroe
Investigation: Z. Pastore, N. S. Church, A. Michels, G. W. ter Maat, R. B. Larsen

Abstract The Seiland Igneous Province (SIP) is a large province of mafic and ultramafic (UM) complexes interpreted to be relics of a giant plumbing system feeding the Ediacaran Central Iapetus Magmatic Province. The Reinfjord Ultramafic Complex (RUC) is one of the four major ultramafic complexes of the SIP. The RUC has a younger dunite core surrounded by wehrlite and lherzolite embedded in country rocks consisting of layered gabbros with sub-horizontal layering and metamorphosed sedimentary rocks. Here, we develop a 3D subsurface model for the RUC using high-resolution magnetic and gravity data and extensive petrophysical measurements from oriented surface samples and drill core samples. Our model indicates that the RUC narrows in depth, extending a minimum of 1.4 km below sea level, and plunges eastwards below the country rock. This model allows us to decipher the lithologic heterogeneities, and the depth and lateral extent of ultramafic rocks, which we interpret in the context of the geologic history of the area. The RUC is spatially separated from other UM complexes of the SIP and the result of this study indicates a smaller depth extent. Combining these findings with the previously reported distribution of the SIP rocks based on the regional gravity data, we propose that the uplift of the crustal block hosting the RUC is larger than for ultramafic complexes in the northwestern part of the SIP.

Plain Language Summary Worldwide, mafic and ultramafic intrusions are considered potential hosts for economic Ni-Cu and platinum group elements. Magma-conduit systems are particularly interesting for such mineralization, because they provide an ideal environment for the formation of large economic sulfide occurrences such as the Norilsk Talnakh deposits. We investigate one of the ultramafic complexes of a large magmatic province considered to represent a deep root zone where transient melts passed en route to upper crustal levels. The RUC is an ideal magma-conduit system for research of large igneous provinces. Here, we construct a subsurface model of the ultramafic complex using gravity and geomagnetic field data constrained by petrophysical data sets from rock samples. We identified the different mafic and ultramafic units, and the alteration of rocks linked to later tectonic events. The localization and the estimation of relative volumes of altered and unaltered mafic and ultramafic rocks provide information about the geodynamic history and the ore potential of these rocks.

1. Introduction

The Ediacaran Seiland Igneous Province (SIP) is a 5,500 km^2 igneous complex of mafic and ultramafic intrusions exposed within the Middle Allochthon of the Norwegian Caledonides. Previous studies have suggested that the SIP could represent a deep segment of a magmatic plumbing system of a large igneous province (LIP) related to the formation of the Central Iapetus Magmatic Province (Grant et al., 2016, 2020). Pressure estimates for the SIP are between 0.6 and 1.1 GPa (Bennet et al., 1986; Grant et al., 2016; Griffin et al., 2013) and indicate that the currently exposed rocks of the SIP formed at depths of 25–35 km in the lowermost parts of the continental crust (Larsen et al., 2018; Sørensen et al., 2019). Pastore et al. (2016) modeled the current extent of the SIP using gravity data and estimated a minimum depth of 9 km. This gravimetric estimate combined with the orientation of the igneous layering of the ultramafic complexes dipping at angles of 0°–20° (Larsen et al., 2018) indicate that an extensive part of the SIP lies below the surface. Deep-seated conduits and magma chambers involved in the generation of LIPs are of great interest with respect to the geodynamic processes within the asthenosphere and the lithosphere. However, well preserved rocks from such conduit systems are rarely exposed, making the SIP an

Methodology: Z. Pastore, N. S. Church, C. Fichler, A. Michels, S. A. McEnroe
Project administration: S. A. McEnroe
Resources: Z. Pastore, N. S. Church, C. Fichler, G. W. ter Maat, R. B. Larsen, S. A. McEnroe
Software: Z. Pastore, A. Michels
Supervision: N. S. Church, C. Fichler, S. A. McEnroe
Validation: Z. Pastore
Visualization: Z. Pastore, C. Fichler, A. Michels, G. W. ter Maat, R. B. Larsen, S. A. McEnroe
Writing – original draft: Z. Pastore, C. Fichler, S. A. McEnroe
Writing – review & editing: Z. Pastore, N. S. Church, C. Fichler, A. Michels, G. W. ter Maat, R. B. Larsen, S. A. McEnroe

outstanding area for studying such structures. Additionally, mafic and ultramafic intrusions are considered potential hosts for economic Ni-Cu-Co and platinum group elements (PGE) mineralization. Maier et al. (2001) suggest open mafic-ultramafic conduit systems are particularly interesting for such mineralization due to the repetitive recharge of fertile melts which potentially could form large economic sulfide deposits.

Here we developed a geophysical and geological model of the Reinfjord Ultramafic Complex (RUC), one of the four major ultramafic complexes of the Seiland Igneous Province (Figure 1). Previous studies indicated that sulfides are present throughout the RUC (Iljina, 2011a, 2011b; Larsen et al., 2018, 2019; Schanche et al., 2012). An electromagnetic survey (skyTEM) in 2011 identified a Ni-Cu-PGE deposit located 80–100 m below the surface of the Central Series dunites (Iljina, 2011a, 2011b; Schanche et al., 2012). This discovery led to the drilling of four exploratory cores (Figure 1b) with depths ranging from ≈120 to 400 m. The high-resolution electromagnetic and magnetic helicopter survey was followed up with ground magnetic and gravity surveys, and geological sampling.

Extensive petrophysical data (ter Maat et al., 2019) from oriented surface samples and unoriented samples from two deep drill cores (R3 and R4) were used here to investigate the subsurface geometry of the RUC by combining 3D gravity and magnetic modeling with petrology and structural information. The gravity method is well suited for detecting the density contrast between the ultramafic rocks and the gneissic and gabbroic country rocks, and for investigating the distribution of these rocks at depth. Magnetic methods help refine this distribution particularly between rock units exhibiting magnetic property variations (ter Maat et al., 2019). Furthermore, the RUC peridotites are locally serpentinized and potential-field methods can be used to map and quantify the extent of serpentinization when this process causes significant contrast in magnetic and or density properties with the unaltered ultramafic rocks. Serpentinization of olivine and pyroxene will reduce the density of the protolith rock and produce magnetite (Evans et al., 2013), which results in an increase in magnetic susceptibility. The magnetic susceptibility does not increase linearly with the degree of serpentinization, and according to Oufi et al. (2002) and Bach et al. (2006) the amount of magnetite formed peaks when >60%–70% of the peridotite is serpentinized; nevertheless, small variations in magnetite content can be quantified using magnetic property measurements. Here we developed a 3D model of the RUC to constrain the extent of the ultramafic rocks which are the potential host for economic mineralizations and, to identify areas of alteration. Furthermore, the RUC is spatially distant from the other major UM complexes of the SIP and we evaluated the derived architecture of the RUC in the larger framework of the SIP.

2. Geological Setting

More than 17,000 km^3 of igneous melts intruded into the deep crust at ca. 580–560 Ma forming the Seiland Igneous Province (SIP), the largest complex of mafic and ultramafic intrusions in northern Fennoscandia. The SIP is located within the Kalak Nappe Complex (KNC), a part of the Middle Allochthon of the North Norwegian Caledonides. The SIP formed during extensional rifting (Roberts et al., 2010) and is considered to represent the deep section of an igneous plumbing system, accommodating thousands of km^3 of dense mafic and ultramafic magmas (Grant et al., 2016; Larsen et al., 2018). Petrological and geochemical data indicate that the SIP intruded in multiple stages over a short time interval (Bennet, 1974; Bennett et al., 1986; Roberts et al., 2010).

There are four major ultramafic complexes within the SIP (Figure 1a): Melkvann and Nordre Brumandsfjord exposed on the island of Seiland, the Kvalfjord intrusion on the island of Stjernøya, and the RUC on the Øksfjord peninsula. Smaller complexes are found both in Øksfjord (i.e., Tappeluft) and Stjernøya. The RUC is in the southwestern part of the Øksfjord peninsula, and the exposed outcrop covers an area of 12 km^2. According to Larsen et al. (2018), the RUC features a deeper section of the magmatic conduit system than the other ultramafic complexes in the SIP.

A modified geological map of the RUC by Grannes (2016) is shown in Figure 1b. The RUC formed from three major pulses of ultramafic magma (Emblin, 1985) leading to the formation of three series: the lower layered series (LLS) consisting of lherzolites and wehrlites, the upper layered series (ULS) consisting of wehrlites (Figure 1d), and the central series (CS) composed mainly of dunite (Figure 1c). These series formed from progressively more primitive magmas throughout a reversed fractionation sequence (Grant et al., 2016). Rocks from the RUC are well preserved with minimal alterations of their original magmatic features. Local areas show a variable degree of serpentinization, commonly related to fluids associated with faults. According to Emblin (1985), along the Storvannet valley a major E-W trending fracture zone (F1 in Figure 1b) has allowed for extensive

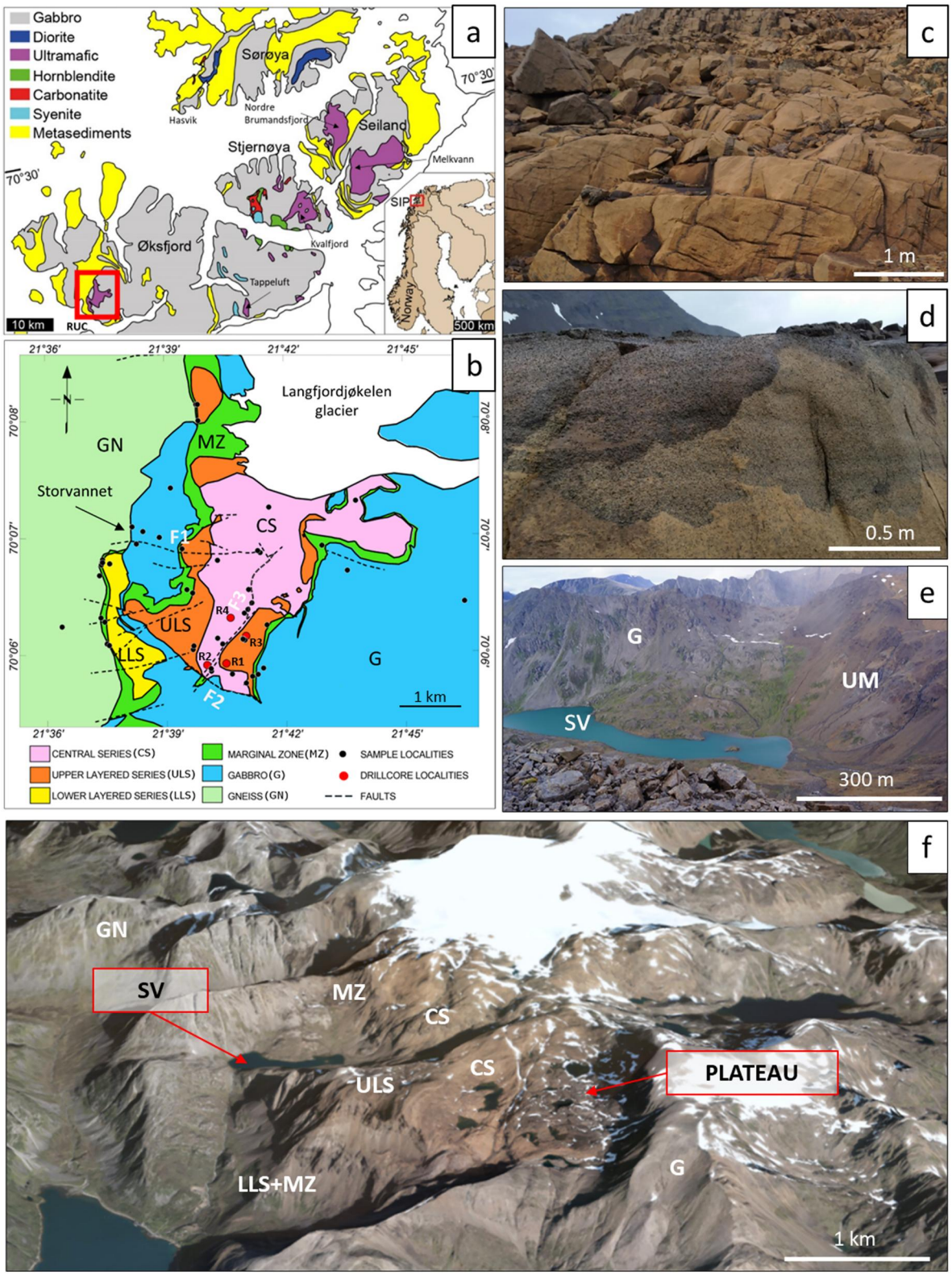

Figure 1.

serpentinization. The SE-NW striking fault (F2 in Figure 1b) shows little to no serpentinization compared to the Storvannet faults (Grannes, 2016). This fault separates the ultramafic rocks from the gabbro and may partially be a synmagmatic boundary fault forming during emplacement of the RUC forming melts. The lack of serpentinization observed in this area may be related to a low permeability for late fluid flow compared to the northern E-W striking fault near Storvannet because this fault was sealed during solidification of the RUC (Grannes, 2016). Additionally, a NE-SW fault passes through the center of the RUC (F3 in Figure 1b) and is associated with narrow serpentinization zones (<1 m). This fault is thought to be synmagmatic and the localized serpentinization to relate to magmatic volatiles (Sørensen et al., 2019).

The country rocks of the RUC are gabbros with sub-horizontal layering and metamorphosed sedimentary rocks (Figures 1b, 1e and 1f). Mapped along the contacts between the ultramafic rocks and the country rocks are marginal zones (MZ), consisting of hybrid rocks formed by partial melting and assimilation of host rock by the RUC-forming melts. These rocks have variable amounts of plagioclase, olivine, pyroxene, and minor oxides.

The RUC is well exposed with little or no vegetation. Except for the LLS and the MZ in the SW margin of the RUC, the ultramafic rocks are exceptionally well exposed, particularly on the plateau (elevation ≈ 600 m above sea level; Figure 1f). The LLS crops out only in the southwestern part of the RUC and is separated from the ULS by a thin screen of gabbro. The lack of direct contact between the different layered series results in some uncertainty on the intrusive relation between the two. The CS dominates the central and the eastern parts of the RUC and is characterized mainly by dunite with subsidiary wehrlite.

3. Geophysical Data

The geophysical data used for modeling the RUC include high-resolution aeromagnetic data (Figures 2c and 2e) and land gravity data (Figure 2d).

3.1. Magnetic Data

SkyTEM Surveys ApS carried out a high-resolution helicopter magnetic survey along EW-oriented flight lines, spaced 50 and 100 m, with nominal terrain clearance of 30–40 m (Johnson & ASA, 2011). Figure 2c shows the map of the total magnetic intensity (TMI) corrected for the International Geomagnetic Reference Field (IGRF: 11th generation; Finlay et al., 2010) ranging from −1497 nT to 2078 nT (SkyTEM Surveys report, 2011). The elongated magnetic low observed along the faults in the Storvannet area reaches its highest intensity of −1497 nT (below background) at the contact between the ULS and the CS (Figures 2a and 2c). The LLS and the MZs in the southwest correspond to a magnetic anomaly low with a maximum amplitude of ≈1000 nT below background. Locally, magnetic lows are observed in the plateau area (south of the Storvannet valley) within the CS, and in the ULS to the east. Here, the average magnetic intensity is approximately −500 nT and reaches an intensity of ≈−745 nT close to drill core R4. Magnetic highs occur above the gabbros to the east of the RUC (with a maximum magnetic intensity of 1791 nT), and at the contact between the MZ and the gabbro to the west, where the intensity reaches 2078 nT. The magnetic anomalies show some correlation with topography (Figure 2b). Scattered mafic and ultramafic dikes are observed throughout the entire CS. These dikes are particularly dense on the hill, north of the plateau area (Figures 2a and 2e). At this location, the dike swarm covers an area of ≈1 km^2 (Orvik et al., 2019) and correlates with a local TMI increase of ≈200 nT observed in the aeromagnetic anomaly map (Figure 2e).

3.2. Gravity Data

Gravity data were acquired with a LaCoste and Romberg G-569 gravimeter; data point locations are shown in Figure 2d. During the survey, base stations were visited twice a day, and differences in the observed readings were used to construct a linear drift function for each day which was subtracted from the data. The maximum drift correction based on repeated base station measurements was ≈0.4 mGal, except for the last day of survey where

Figure 1. (a) Geological map of the SIP (modified after Larsen et al., 2018). The location of the RUC is outlined by the red box. (b) Geological map of the RUC (modified after Grannes, 2016 and Sørensen et al., 2019) with locations of sample sites and deep drill cores (ter Maat et al., 2019). Outcrop photographs of the central series (c), layered series (d), the Storvannet Valley (SV) with the gabbro (G) and the ultramafic rocks (UM) (e). F3 is based on Ryan et al. (2022). (f) 3D view from south (©norgeibilder.no, www.norgeibilder.no, Finnmark 2015, Omløpsfoto), note the marked contrast in color between the ultramafic rocks (dark brown), and the country rocks (gray).

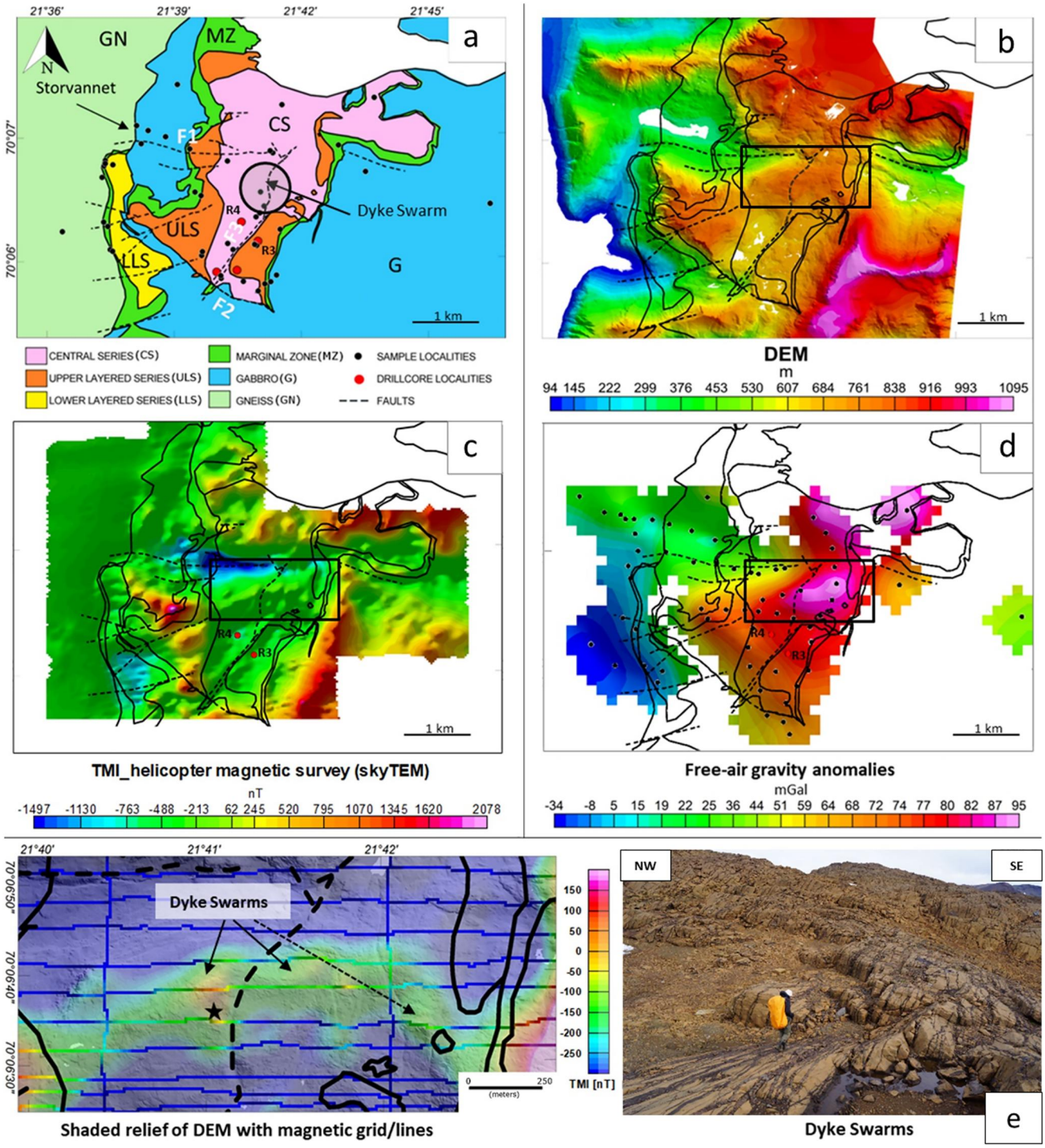

Figure 2. (a) Geological map of the RUC with samples localities and main faults. Boundaries of lithological units are superimposed on the geophysical maps. (b) Digital Elevation Model - DEM (airborne LiDAR data/Norwegian Mapping Authority at https://hoydedata.no). (c) Shaded relief map of TMI anomalies. (d) Shaded relief map of free-air gravity anomalies (ground survey) with gravity acquisition points (black dots). (e) Enlarged view of the magnetic anomalies over the dike swarm area (black box in Figures (c) and (d)) on top of a shaded relief image of the DEM. Two grids of the magnetic data are shown in the map with the same stretched linear color scale, one is produced with a blanking distance of 100 m, the other with a smaller blanking distance of 5 m to highlight the data coverage along the flight lines with respect to the size of the dikes, which are shown in the field photo to the right.

the maximum drift was estimated to ≈3 mGal. Elevation was measured in the field with a handheld Garmin GPS 64th, with positioning accuracy of 3 m in horizontal direction and approximately 10–15 m in vertical direction, which was calculated by comparison to the LiDAR elevation data yielding an accuracy of ±1 m. This gives an uncertainty of approximately 3–5 mGal to the measured gravity data. Each gravity measurement was corrected for the gravity field given by the International Gravity Formula 1980, and the free-air correction (Blakely, 1996) was applied. Although the free-air gravity anomalies include the effect of the masses interposed between sea level and station elevation, we did not consider using the Bouguer gravity corrected data for modeling due to the high variability of densities across the complex. Instead, we chose to model the entire subsurface to account for the full gravity effect of the masses in the subsurface.

4. Petrophysical Data

During the 2014 and 2015 field seasons over 300 oriented samples were collected from 48 sites in the RUC. These sites and the deep drill core locations are plotted on Figures 1b and 2a. Later samples were cut into specimens (2.2 cm long and 2.5 cm in diameter) and measured for density (667), NRM (651) susceptibility (649). This data was compiled by ter Maat et al. (2019) and are used here to constrain the geophysical interpretation.

4.1. Density and Magnetic Susceptibility

Samples were collected from all units in the RUC. In Figure 3 the site average densities (Figure 3a) and magnetic susceptibilities (Figure 3b) are plotted on the magnetic anomaly map (TMI). The petrophysical properties of each sampling site were calculated by averaging several specimens (2–31, see ter Maat et al. (2019) for specimen and site properties). For the two deep drill cores averages for the units were calculated over a larger number of specimens (13–78) depending on the thickness of the unit along the core. The country rocks surrounding the ultramafic complex consist of gneiss and gabbro. The gneiss bounds the complex to the west and has an average density of 2,710 kg/m^3. The gabbros are exposed on both sides of the complex and have average densities of 3,010 kg/m^3 with slightly lower densities for the gabbros to the east compared with those to the west of the ultramafic complex (Table S2 in Supporting Information S1). Due to variations in magnetite, ilmenite, hemo-ilmenite, and sulphide content, the magnetic susceptibility of the layered gabbro ranges from 0.0002 to 0.071 SI with a median of 0.014 SI (ter Maat et al., 2019). The average magnetic properties at each site show a correlation with the magnetic anomaly map (Figure 3b). However, the correlation between magnetic anomalies and the mapped lithological units is poor, which indicates some variation in mineralogy within the units.

In particular, the deviating densities and magnetic susceptibilities at the Storvannet valley correlating with the magnetic low (black dashed box in Figures 3a and 3b), reflect a change in bulk chemistry due to serpentinization (ter Maat et al., 2019). Considering the current direction of the inducing geomagnetic field (9° Declination and 78° Inclination), and the high magnetic susceptibility (0.02 SI–0.05 SI), a magnetic high is expected. However, here there is a distinct magnetic low (below background) indicating that these rocks must contain a component of remanent magnetization with a higher intensity than the induced magnetization, and with different direction from that of the present-day geomagnetic field. The degree of serpentinization of CS samples from the Storvannet valley varies from 58% to 95%. Outside of the Storvannet valley, most of our surface samples of the ultramafic rocks show only minor alteration in thin sections and 70% of the surface ultramafic samples of the RUC have limited alteration with serpentinization degree in the range 0%–20% (ter Maat et al., 2019). The rocks from the southern part of the CS, the LLS, and the deep drill cores (R3, R4) also have high densities, with site average densities between 3,230 and 3,376 kg/m^3. Figure 3c shows the localities of the drill holes R3 and R4 (Grant et al., 2016) and a log of their densities and susceptibilities (ter Maat et al., 2019). Samples from the drill cores have limited to no alteration (Figure 3c) and 70% of the samples show a maximum degree of serpentinization of 10%. The densities of the ultramafic rocks from the drill cores range between 2,790 and 3,394 kg/m^3 with a median density of 3,265 kg/m^3. Local segments of low density, which are correlated with high magnetic susceptibilities commonly >0.01 SI, are caused by the occurrence of serpentinite veins. However, this correlation is not always observed along the serpentinized segments of the drill core logs (Figure 3c) due to local changes in the modal composition of the rock. Despite the visual evidence of serpentinization along the core, local occurrences of sulphides and/or small pyroxenite or gabbroic veins within the CS can increase or decrease the density of the rock without measurably influencing the magnetic susceptibility. High densities and magnetic susceptibilities are observed in samples from the marginal zone at the

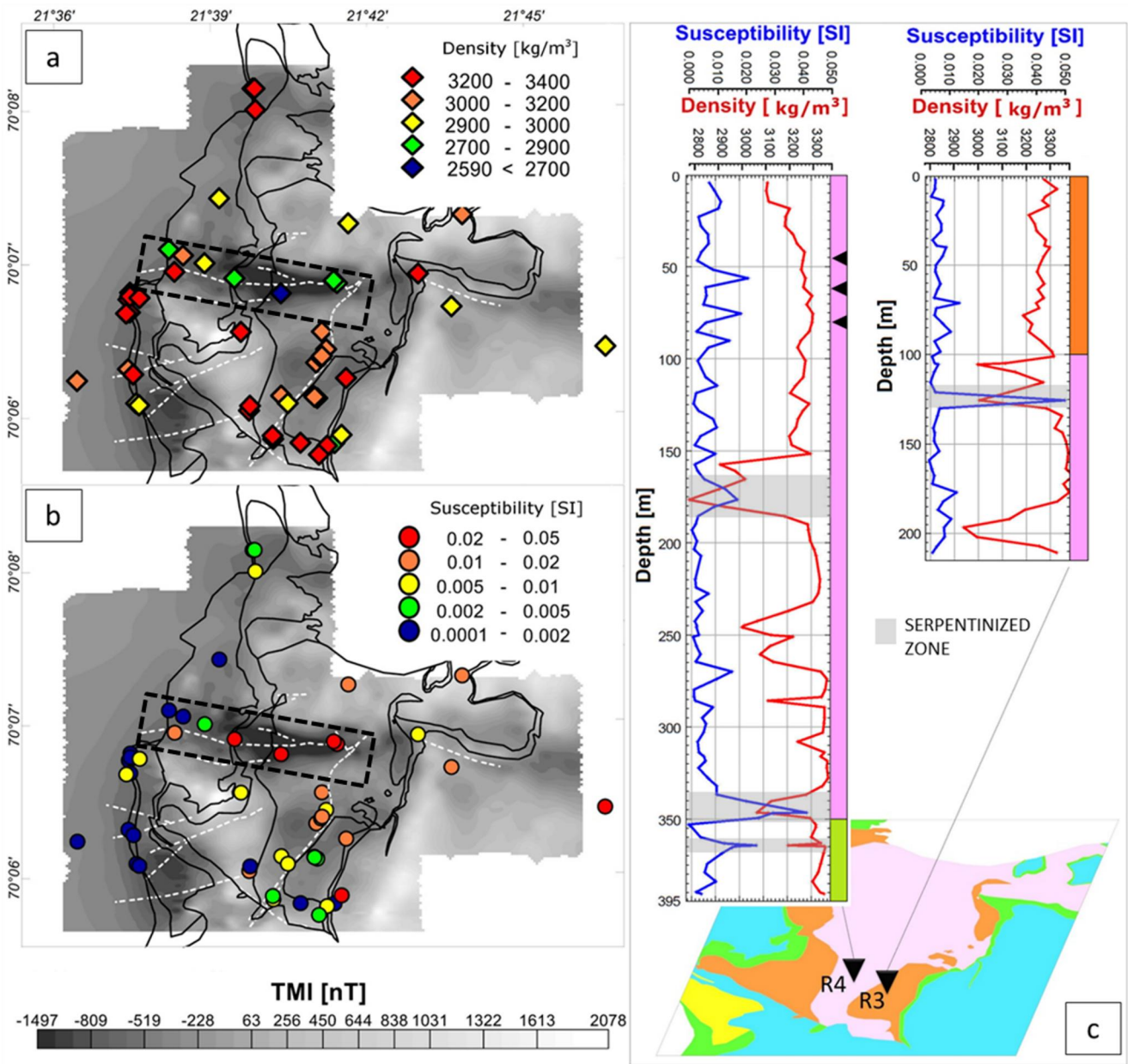

Figure 3. Average densities (a) and magnetic susceptibilities (b) for surface samples superimposed on the aeromagnetic map with lithological boundaries (black lines) and area of Storvannet valley (black dashed box). (c) Deep drill cores densities and susceptibility logs (ter Maat et al., 2019) and geological map with localities for the deep drill cores R3 and R4 (see Figures 1b and 2a for geological map legend). Black triangles on the R4 lithology-log indicate increased concentrations of Cu and PGE (Larsen et al., 2018). Highlighted in gray bands are serpentinized regions based on the drill-core logs. These coincide with both lower density and high susceptibility. Areas with decreased density but with low susceptibility could be due to carbonate veins in the dunite.

contact between gabbro and ultramafic rocks (ter Maat et al., 2019). Site averages of susceptibilities at these localities range between 0.007 SI and 0.02 SI. Rocks from the marginal zones are typically characterized by coarse-grained (up to 1–2 cm) pyroxenites (Grant et al., 2016) with variable amounts of olivine, plagioclase and minor sulphides, magnetite, ilmenite, and rutile.

4.2. Natural Remanent Magnetization (NRM) and Koenigsberger (Q) Ratios

The in situ magnetization of rock bodies is the vector sum of two components, the induced magnetization (Ji), which exists only in the presence of an external magnetic field, and the remanent magnetization, that remains even

in the absence of such a field. The direction and intensity of these components is essential to correctly model and interpret the magnetic anomalies. The ratio between the NRM and the induced magnetization (Ji) is called the Koenigsberger ratio (Q) and is calculated by:

$$Q = \frac{NRM}{JI} = \frac{NRM}{\text{magnetic susceptibility} \times H} = \frac{NRM}{\text{magnetic susceptibility} \times \frac{B}{4\pi \times 10^{-7}}}$$

The induced magnetization is calculated as the product of the magnetic susceptibility of the sample and the value of the geomagnetic field intensity, which for this locality is B = 53,412 nT or H = 42.5 A/m. Here, we refer to "Qs" to indicate that the ratio is calculated using the vector sum of the NRMs at the site level (Table S1 in Supporting Information S1). For all site locations, the Qs ratios, and directions of NRM, induced magnetization and resultant magnetization (vector sum of Ji and NRM) are plotted on Figure 4 with arrows. The length of the arrows is proportional to the total intensity of the magnetization and the arrow direction indicates its inclination. The map in Figure 4 provides a qualitative comparison of the magnetization of samples across the RUC and for simplicity, the declination is not shown. However, variations in declination are discussed in the modeling section.

NRM and Ji intensities vary across the complex, and 68% of the sites Qs ratios lie between 1 and 4 (Table S1 in Supporting Information S1). In the CS, particularly high NRM intensities are measured in samples from the magnetic low east of the Storvannet Lake, and in the northern part of the CS. High NRMs occur also in gabbroic samples on the eastern side of the ultramafic complex, and in the samples of the MZ. The highest NRM intensity value (26 A/m) is from a pyroxenite dike sample of the ULS, in the southwestern quadrant of the complex. Pyroxenite samples contain abundant magnetite and ilmenite exsolution lamellae in the pyroxenes (ter Maat et al., 2019). Other areas of dense pyroxenite dikes (Figure 2e) have been recognized in the field within the CS just south of the Storvannet magnetic low, which is at the northern end of the plateau area. Generally, in the RUC, Qs ratios are above 1 (Figure 4 and Table S1 in Supporting Information S1), indicating that NRM contributes to the magnetic anomalies. Particularly high Qs ratios ($Q > 8$) occur in the MZ at the boundary between gabbroic and UM units.

The present geomagnetic field at the RUC has a steep inclination of 78°. Mean vector NRM inclinations of most RUC rock units (Figure S3 in Supporting Information S1) are positive and therefore, the NRM vector component should broadly add to the induced magnetization component. However, NRM site vector average inclinations range from −37° to 84° (Table S1 in Supporting Information S1) locally influencing the magnetic anomaly pattern. Due to the high coercivity of the samples we do not expect a large component of the NRM to be due to a viscous remanent magnetization (VRM) (ter Maat et al., 2024). In Figure 4, the longest arrows for the resultant magnetization vectors correlate with areas of magnetic anomaly highs. Samples from the prominent Storvannet magnetic low area have NRM intensities above 3 A/m and inclinations that are shallower compared to other sample localities in the RUC with values between −2° and 50°, deviating from the current geomagnetic field direction. NRM directions and intensities in the gabbro show a wide variation and are different on the sides of the ultramafic complex (Figure 4). Locally, some gabbro samples have negative to shallow NRM inclinations, high magnetic susceptibilities above 0.01 SI and Q ratios above 3.

NRM and susceptibility values are the combined effect of the concentration, composition, grain size and textures of the magnetic minerals (McEnroe et al., 2001, 2007, 2009a, 2009b; Robinson et al., 2016). Paramagnetic minerals such as olivine, pyroxene and pure ilmenite have very weak magnetic susceptibility, and do not carry a magnetic remanence. Below their Curie temperature, ferrimagnetic minerals such as magnetite have a high magnetic susceptibility and carry an NRM (Clark, 1997); such minerals can dominate the magnetism of rocks and their properties are important in the interpretation of magnetic anomalies. Figure 4 shows microscopy images of a weakly magnetic dunite sample (Figure 4a) in comparison with two strongly magnetic serpentinized dunite samples (Figures 4b–4d). The serpentinized samples contain magnetite in μm-thick veins and as discrete large grains. With the formation of serpentine at the expense of the olivine, these altered samples have lower densities than the pristine dunite sample. The gabbros from east and west sides of the ultramafic complex are magnetically distinct and, this is reflected in the observed mineralogy: the gabbro from the western side (Figure 4e) contains hemo-ilmenite but lacks magnetite, while the gabbro from the eastern side additionally contains magnetite (Figure 4f).

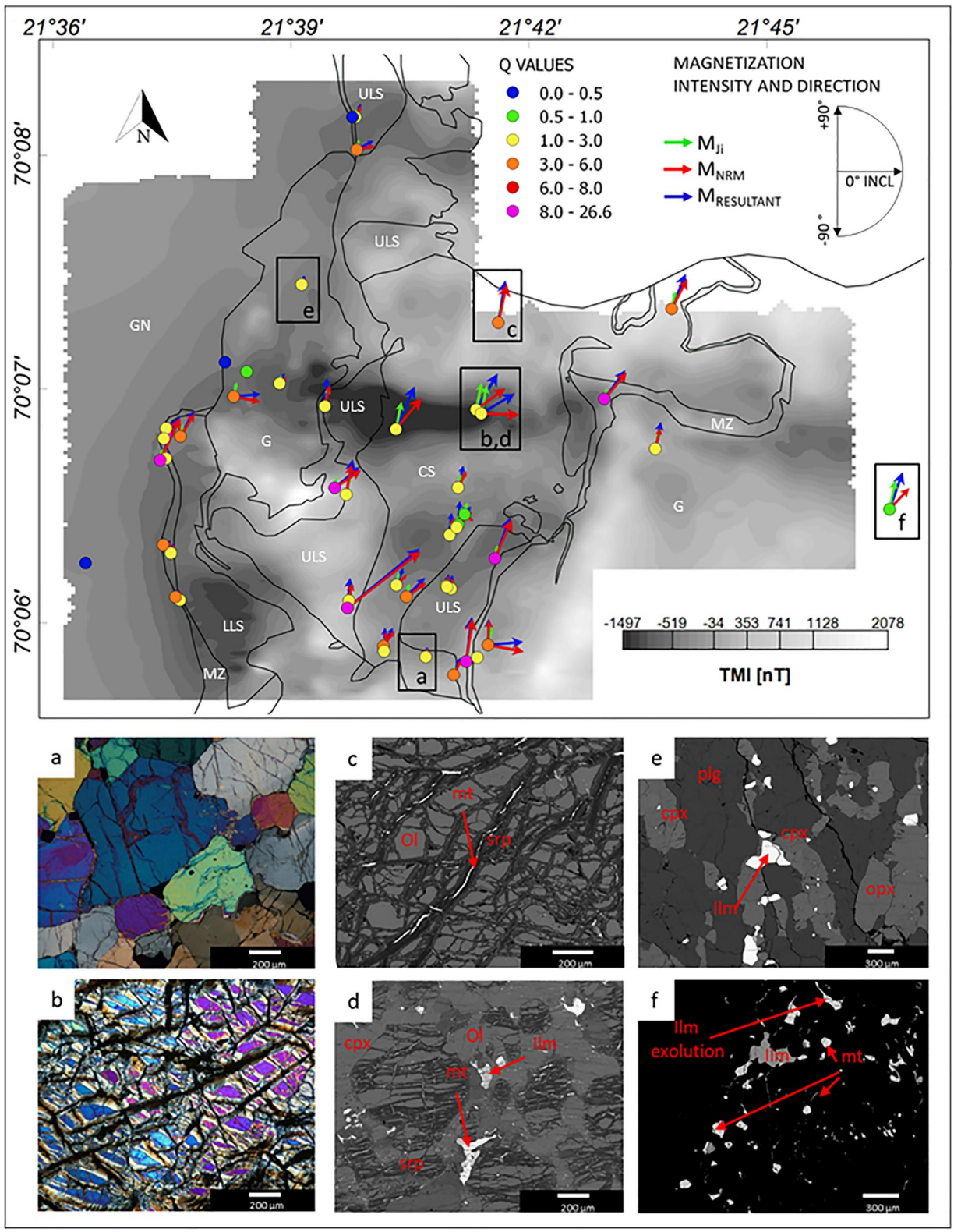

Figure 4.

5. Modeling Results

5.1. 3D Gravity and Magnetic Model

To investigate the sources of gravity and magnetic anomalies, we developed a combined 3D gravity and magnetic model. Physical properties used in the gravity and magnetic model were selected based on statistical analysis of surface sample properties in the shallower part of the model and deep drill core properties in the deeper part of the complex (Table S2 in Supporting Information S1). Site densities and susceptibilities were averaged, while site NRM directions were calculated by vector averaging. Statistics for NRM mean directions were calculated at both site (Table S1 in Supporting Information S1) and unit level (Table S2 in Supporting Information S1) to account for the range in properties within a lithological unit. A stereonet of the NRM directions of the ultramafic rocks shows that the mean vectors for all units, except for the CS serpentinites, have steep positive inclinations (Figure S3 in Supporting Information S1).

A 3D subsurface model was constructed using Tensor Research Pty Ltd Encom ModelVision™ software version 17.5 (Oldenburg & Pratt, 2007; Pratt et al., 2006) and Geosoft Oasis Montaj™ was used for map visualization. The gravity and magnetic fields calculated from the forward model were required to match the measured gravity and magnetic data at each station. The subsurface model was constructed along 12 parallel NW-SE oriented cross-sections and with polygonal prisms which fill the entire subsurface (Figure 5). The orientation of the cross-sections was selected to be perpendicular to the lithology contacts. The polygonal bodies seen on profile are cross sections of prisms with defined strike direction and lateral extension. The modeling process allows for interactively changing the edge points of the polygons along cross-sections and the prisms' properties. In the map plane, it is also possible to change azimuth and strike length of the prisms. To avoid overlap of the prisms we used the same strike direction for all bodies. Major steps between the prisms will cause edge effects in the calculated gravity and magnetic data. This effect is minimized by having the data points in the center of the surface-facing part of the prisms.

This modeling style allows for complex lithological unit geometries observed in the RUC and large variability in petrophysical properties that yields the complex magnetic anomaly pattern. Several of the lithological units were made up of multiple polygonal bodies to reflect local variability and to incorporate information from surface samples. Although the model is relatively complex and there are many degrees of freedom, we evaluated alternative options in the range of the measured petrophysical properties and focused on the following aspects of the model which are important for the mineralization potential, and for the tectonic history of the complex: (a) contacts between mafic and ultramafic units, (b) the minimum depth extent of the ultramafic rocks, (c) relative volumes of altered and unaltered ultramafic rocks.

The locations of the cross-sections are shown in Figure 5 and are superimposed on geological, aeromagnetic, and free-air gravity anomaly maps. To avoid edge effects due to the finite size of the model, the body representing the model background extends well outside the target area to cover an area of 100 × 100 km. As seen on the geological map (Figure 1b), the gabbro that bounds the complex extends for tens of km toward the northern and the eastern side of the complex. In the model the gabbro has been extended laterally on the eastern side of the mapped ultramafic rocks (2.5 km outside the modeled profiles) and on the northern and southern side of the modeled area. Figure 5 shows the model that best agrees with the potential-field data and the geological constraints which include surface lithological contacts, petrophysical properties and previous electromagnetic models. Alternate model scenarios are discussed in the next section. The preferred model suggests the RUC extends to a depth of 1.4 km (Figure 5a) with the deepest section to the northeast. The ultramafic complex

Figure 4. Top: Aeromagnetic anomaly map with Qs ratios (circles) and site average magnetization vectors (arrows). The length of the arrow is proportional to the square root of the magnetization intensity (the magnetization intensity varies over several order magnitudes, therefore we plotted the square root of the magnetization intensity rather than the magnetization), while the arrow direction shows the inclination of the magnetization (0° inclination with arrow pointing toward east, and 90° inclination with arrow pointing toward north). Samples with magnetization lower than 0.1 A/m do not have the arrows plotted. Though the gabbro bodies bounding the UM rocks have similar Qs ratios (1–3), the eastern gabbro has significantly higher susceptibility and NRM values. Bottom panel: Optical and backscattered electron images (BSE) of samples with locations marked on top panel by black boxes. (a) Optical image of a CS pristine dunite sample. (b), (d) Optical and electron images of CS serpentinized samples from the Storvannet magnetic low area which contain magnetite (mt) both in serpentine (srp) veins and in larger grains (>50 μm). (c) Backscattered electron image of a serpentinized sample from the northern part of the CS. (e) BSE image of a gabbro sample from the western side of the ultramafic complex with plagioclase (plg), orthopyroxene (opx), clinopyroxene (cpx), ilmenite with hematite exsolution lamellae (Ilm) and rutile. (f) BSE image of eastern gabbro contain both magnetite and ilmenite.

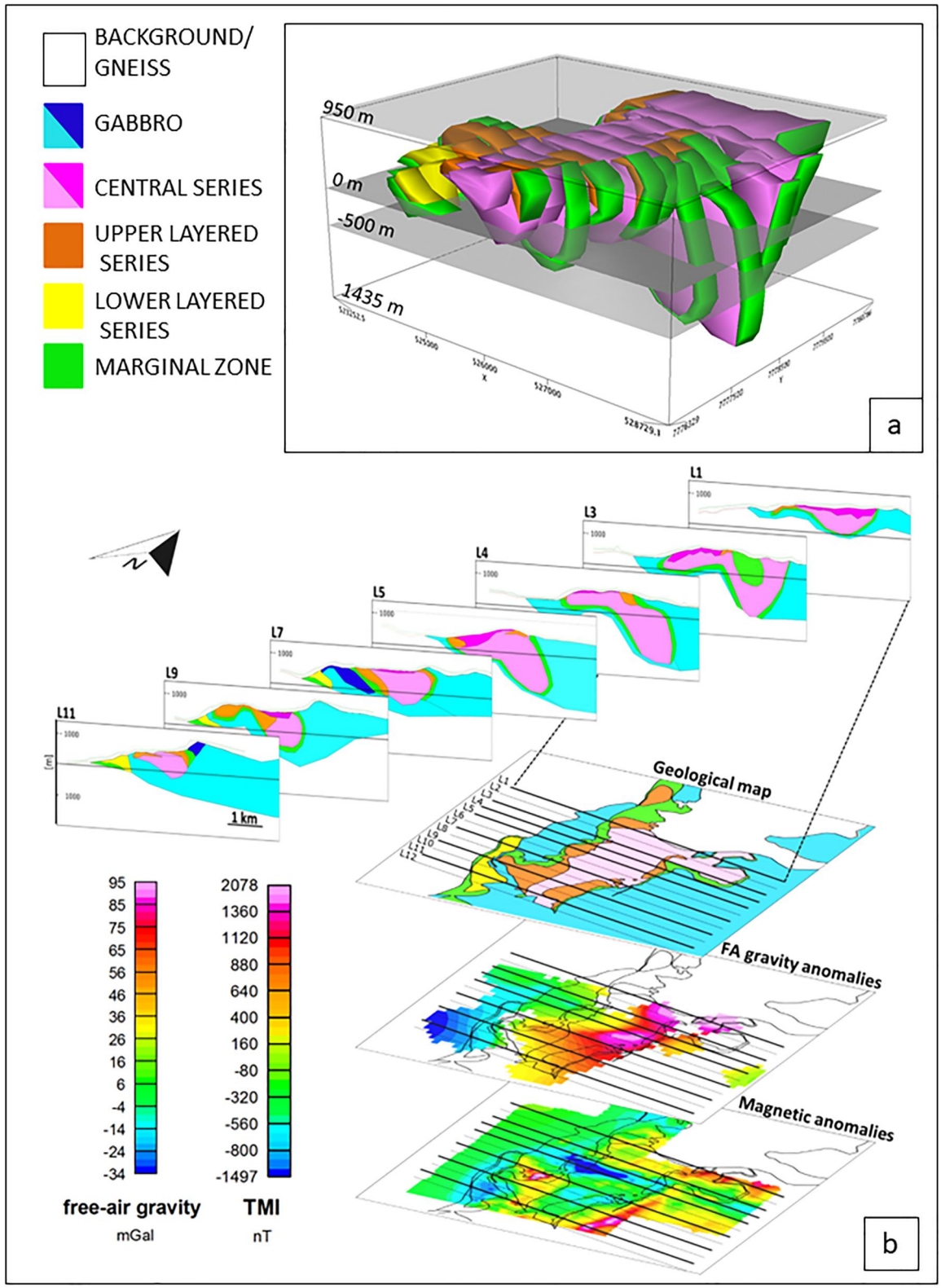

Figure 5. (a) 3D model of the RUC with central series (CS), upper layered series (ULS), lower layered series (LLS) and marginal zone (MZ). Zero delimits sea level. (b) Multi-profile-based 3D model with selected cross sections, and their locations shown on geological, free-air (FA) gravity and aeromagnetic maps. The displayed cross sections are marked by bold black lines with line numbers on the geological map.

becomes shallower toward west and south. In particular, the CS is deeper on the eastern side with its maximum extension below the gabbro on the northeastern part of the complex.

Although the Central Series has a thickness of 800 m in cross-section L1, the gravity data is limited to one acquisition point on the eastern side of the section leaving uncertain the depth extent of the CS and of the gabbro. Gravity data points intersecting the adjacent cross-section L2 display a lower gravity signal on the western side of the complex which leads to a drastically reduced thickness for the intrusive rocks at the contact with the gneiss. The ultramafic part of the complex widens in the next sections reaching a depth of 1.3 km in L3, and of 1.4 km in L4. In these sections the upper part of the CS is modeled with a higher magnetization compared with the deeper part (Figure 6). Thin-section observations (Figure 4c), and petrophysical measurements support the interpretation of an increase in alteration of the ultramafic bodies at and near the surface, leading to enhanced magnetization. In L4, the MZ and at greater depths, the CS continue below the gabbro on the eastern side, suggesting a continuation of the ultramafic rocks at depth toward east. This continuation is constrained by the higher gravity signal observed on the eastern side of the UM complex, and by the short-wavelength magnetic anomaly occurring in the adjacent gabbro which is interpreted to be due to the dipping MZ below the gabbro. Cross-sections L5 and L6 cross the Storvannet valley to the west, which is associated with the magnetic low down to −1497 nT. The modeled serpentinized zone of the CS along the cross-section L5 has a thickness of 400 m, a magnetic susceptibility of 0.05 SI, and an NRM with negative inclination (Figure 6). The main magnetic carrier in these samples is endmember magnetite which formed during serpentinization (Pastore et al., 2018). The magnetite formed by this process acquired a chemical remanent magnetization (CRM) later than the primary thermoremanent magnetization (TRM) acquired during the cooling of the complex. Given the shallow to negative inclinations of these NRMs, it is likely that the serpentinization occurred during a period of a geomagnetic reversal. In L6, the serpentinized zone within the CS is smaller compared with L5 and limited to the contact area with the ULS. In both cross sections, the CS dips toward east and is bounded by the MZ. The underlying MZ is interpreted to contribute to the magnetic high occurring within the area of the gabbro rocks on the eastern side (Table S2 in Supporting Information S1). Samples from the gabbro on the eastern side of the intrusions show a range in magnetic properties related to internal layering of the gabbro and locally have magnetic susceptibilities above 0.018 SI (sites 47 and 48 in Figure S1 in Supporting Information S1).

In the northernmost cross sections, the gabbro on the western side is bounded by gneiss. A different geometry is found in both L6 and L7 where the gneissic country rock is separated from the gabbro by the Lower Layered Series (LLS). Along lines L6 and L7, where the LLS outcrops, the gravity anomaly is below 10 mGal. This indicates that the ultramafic rocks forming the LLS with their high average density of 3,300 kg/m^3 do not extend deeper than 400 m at this location. The thin gabbro layer on the western side of the intrusion was modeled along these sections as the uppermost magnetic layer. This layer may have an enhanced magnetization due to a higher content of magnetic oxides, and/or sulfides. The increase in magnetic minerals may be a result of contact metamorphism between the gabbro and the RUC when it intruded at temperatures of at least 1400°C (Bennett et al., 1986; Larsen et al., 2018).

In cross-sections L8, L9, and L10, the thickness of the ultramafic rocks decreases toward the south. The ULS and the LLS are in contact below the surface (Larsen et al., 2019). However, the low gravity signal in this area implies that lower density gabbroic and/or gneissic bodies dominate this area. In these cross-sections the top part of the CS is modeled with negative NRM inclinations similar to the rocks from the Storvannet magnetic low. Although not supported by the available sample database, negative NRM inclinations are required to match the magnetic anomaly lows observed in these areas, which have an average total magnetic field intensity of −500 nT. The modeling suggests that this top part has a thickness of 300 m in L8, where it is at its deepest. CS surface samples in this area are slightly serpentinized with reduced densities between 3,000 and 3,100 kg/m^3. Here, most samples have positive NRM inclinations (Figure 4).

Analyses of cross-sections L11 and L12 indicate a thinning of the CS toward south. The magnetic high at the eastern end of section L11 could not be modeled by a homogeneous gabbro body and was instead modeled with two bodies. The small gabbro body next to the MZ was modeled with higher susceptibility and NRM values.

The modeled and observed gravity and magnetic anomalies are shown in Figure 6 and were calculated by gridding the values modeled along the sections. The modeled anomalies gave a reasonable fit to the observed. Differences between observed and calculated anomalies (residual anomalies) range between −569 and 449 nT, with an average of −40 nT. At the gravity points the differences between the observed and the calculated fields gave

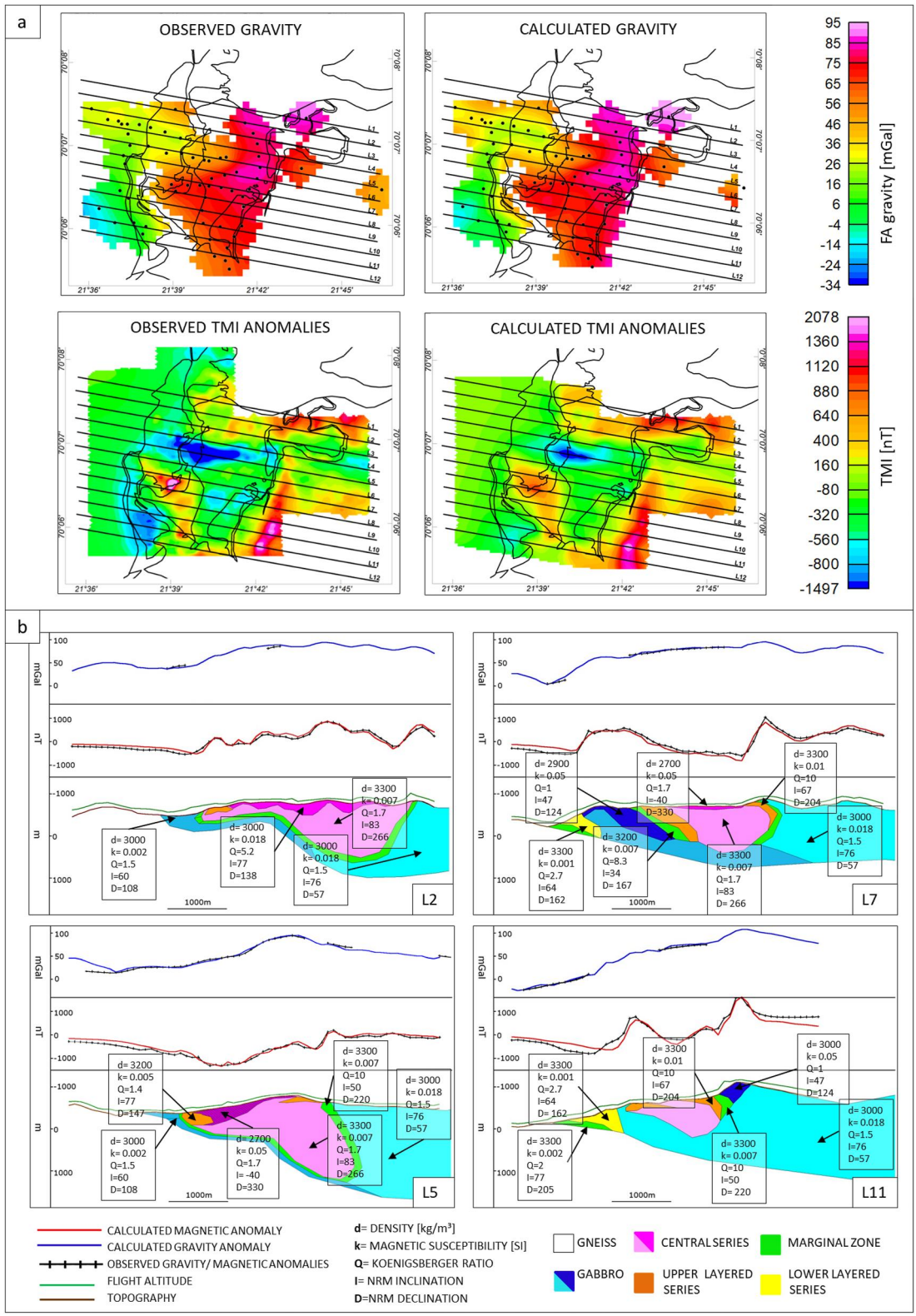

Figure 6. (a) Cross sections L2, L5, L7, and L11 with modeling parameters and calculated and observed free-air gravity and magnetic TMI anomalies. Black dots on the gravity grids are the gravity measurements points, black lines are the modeled cross-sections. (b) Cross sections L2, L5, L7, and L11 with modeling parameters.

residual gravity anomalies in the range of ±5 mGal. Based on the previous considerations on stations' elevation accuracy, the error on the measured gravity field was estimated to 3–5 mGal. Furthermore, a minor error is due to the model structure, as the model is built along cross-sections, and it is only along these cross-sections that the modeled bodies' top surfaces are matched to the topography. Finally, the different spacing of the airborne acquisition flight lines 50 or 100 m and, of the modeled cross-sections of 300 m, results in higher residual magnetic anomalies in the areas between the modeled lines.

5.2. Model Scenarios

Due to the ambiguity of inversions from potential fields, a model that matches the data is not unique; therefore, we tested alternative scenarios, which are shown along the modeling section crossing the Storvannet valley (L5, Figure 7). The models shown in Figures 5–7, are constrained at the surface by lithological boundaries, surface samples properties, and at depth by the densities and magnetic properties of samples from 2 of the deep drill cores (R3, R4). We investigated whether the magnetic anomalies are dominated by NRM, by induced magnetization, or a combination of both. Most of the samples of the RUC have Qs ratios above 1 (Table S1 in Supporting Information S1), therefore, an NRM component will contribute to the magnetic anomalies.

The sensitivity of the model was tested by variations in dip, depth extent and petrophysical properties of the UM complex. Figure 7b shows the effect of changing magnetic properties in the surface rocks from the Storvannet valley on the magnetic anomalies. Samples from this area have shallow to negative inclinations, and high Q ratios. To match the magnetic low, a negative inclination of −40° (Figure 7) was used for these surface rocks, while the deeper part of the CS was assumed to be homogeneously magnetized and weakly magnetic according to the drill core properties (Table S2 in Supporting Information S1). Specifically, CS samples from the drill cores have lower median NRM and susceptibility values (0.38 A/m and 0.005 SI) than the surface samples (1.2 A/m and 0.011 SI, ter Maat et al., 2019). Here, modeling suggests the serpentinized rocks extend to ∼400 m below the surface. Higher NRM intensity, steeper negative NRM inclination or a combination of the two would contribute to the magnetic low and result in a smaller depth extent of the altered zone. As shown in Figure 7b, a decrease of the NRM inclination toward shallower values (0° and 20°) increases the mismatch between the observed and the calculated anomaly. It cannot be excluded that rocks at this location have shallower inclinations; however, to match the magnetic anomaly low, these rocks should have higher magnetization intensities than those measured on serpentinite samples from this area (sites 14 and 15 in Table S1 in Supporting Information S1). The serpentinite samples from the Storvannet valley have highly variable NRM directions with inclinations ranging from −34° to 77°. Michels et al. (2018) reported NRM directions on more than 500 samples from the heavily serpentinized Leka ophiolite complex. The authors found a large variability in the NRM direction and interpreted this variability as an indication of a complicated thermal history with serpentinization occurring over a long period of time. Here, it is also possible that serpentinization occurred over a long time period resulting in variable directions with average site NRM inclinations ranging from −2° to 50°. The modeled serpentinized area is confined at the bottom by weakly magnetic dunite of the CS that compensates for the gravity signal at this locality and thin layers of MZ and gabbro with a sub-horizontal contact with the ultramafic rocks. This agrees with field observations which indicate that magma emplacement occurred along vertical and sub-horizontal weakness zones. An alternative model would have a thicker weakly magnetic gabbro at this locality.

In our preferred model, the UM complex dips eastward below the gabbro (Figures 5–7). The robustness of this interpretation was tested by changing the dip of the UM complex on all sections. The resulting magnetic and the gravity responses are shown in Figure 7c along cross-section L5. Apart from model M1 having a westward dip of the UM rocks, all other models show a reasonable fit to the gravity anomaly. The model M3 gives the best fit to the measured magnetic anomaly at the boundary between the MZ and the gabbro to the east. However, this anomaly could also be explained by locally a more magnetic layer in the gabbro. Consequently, the model M2 with a vertical contact of the UM rocks with the gabbro, cannot be excluded.

Cross sections L4 and L5 cross the ultramafic complex where it extends to greater depth (Figure 5). Figure 7d shows the effect of changing the depth of the bottom of the CS on the gravity and the magnetic anomalies to lower (M3) or higher depths (M1). The deeper part of the CS is weakly magnetic and therefore these changes have only a minor effect on the magnetic anomalies. The most distinct change is observed on the eastern side of the cross-section with a shift of the magnetic response toward lesser or greater values, for a corresponding increase or decrease in thicknesses of the UM complex, respectively. This shift is also observed in gravity anomalies.

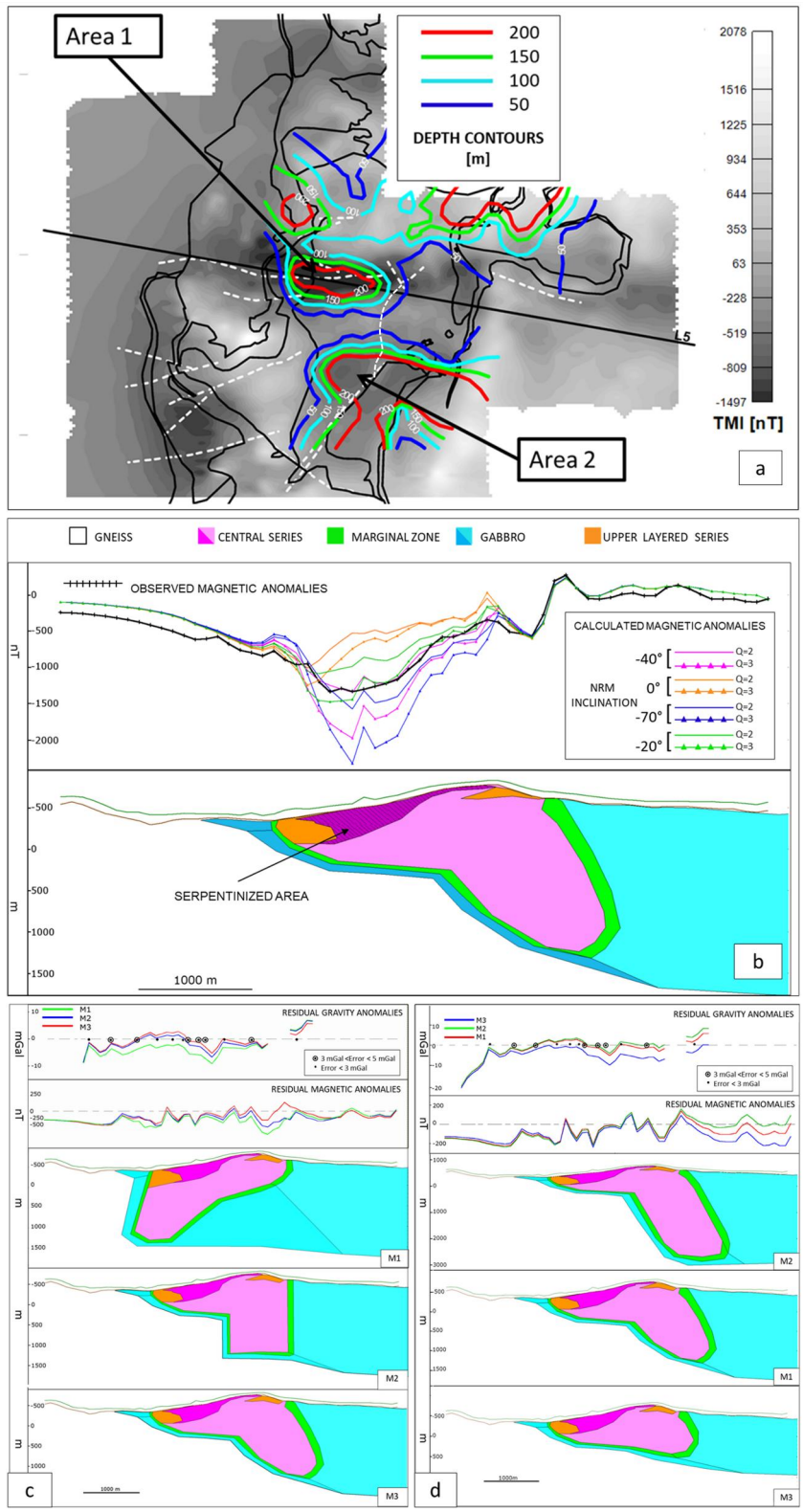

Figure 7.

We set the minimum depth of the complex to 1.4 km as shown in model M2, based on the overall good fit of that model and the maximum reasonable density or magnetization contrast between the ultramafic and surrounding rocks. In the RUC drill core data set, the ultramafic rocks have a maximum density of 3,418 kg/m^3, and mean values of 3,230 and 3,258 kg/m^3 for the CS and ULS, respectively (ter Maat et al., 2019). In our model, the deeper part of the complex is modeled with a density of 3,300 kg/m^3, which is the 75% percentile for the RUC ultramafic rocks. Miller and Christensen (1997) used this value as representative for unaltered peridotite and ultramafic rocks. For the surrounding gabbroic and gneissic rocks, we used the 75% percentile values with densities of 3,000 and 2,700 kg/m^3, respectively. The unaltered ultramafic rocks are weakly magnetic, changing the depth extent of these modeled bodies does not measurably influence the magnetic response at the surface.

However, if the RUC narrows at depth as would be expected for a feeder dike it would not be detectable by the available geophysical data. The acquisition of new gravity data on the eastern side of the complex above the gabbro would help to refine the model and constrain the depth extent better.

6. Discussion

Field data indicates that the RUC was emplaced in multiple magma recharge events resulting in a diversity of bulk compositions and petrophysical properties. The RUC was further modified by later alteration processes. Our modeling results provide an estimate of the buried architecture of the RUC. This is discussed below in relation to petrology, ore potential, and within the larger geological setting frame of the SIP. The model indicates the depth extent of the different lithological units and defines areas of inhomogeneity within each unit based on densities and magnetic properties. In summary, the RUC extends down to a minimum depth of 1.4 km and is deepest in its northeastern part. The observation of multiple recharge events throughout the formation of the RUC, the concentric distribution of its UM rocks with the pyroxene-rich rocks in the marginal parts and olivine-dominated rocks toward the center of the ultramafic complex (Grant et al., 2016; Larsen et al., 2018, 2019), and recent thermodynamic modeling (Grant et al., 2020) support the interpretation of RUC magmas derivation from partial melting of the asthenospheric mantle at 7 GPa (hence depths of >200 km) and argue for a conduit system extending toward greater depths than those estimated here. The lack of a deeper conduit in our model could be explained by (I) a later modification of the structure of the complex with the removal of the deepest part of the root or by (II) an ultramafic conduit that is too narrow to be resolved by the geophysical data. Sensitivity tests suggested that the deeper part on the eastern side of the complex is either near-vertical or is steeply dipping eastward. This agrees well with the mapped surface data. Further, the model suggests that the ultramafic complex is confined with a limited depth in the west and south. Due to the lack of data in the northern part of the study area, which is covered by a glacier, we cannot exclude a continuation of the ultramafic rocks below the Langfjordjøkelen glacier (Figures 1b and 1f).

6.1. Serpentinization

Serpentinization reactions occur in olivine and pyroxene, by the interaction of fluids at temperatures <400°C (McCollom & Seewald, 2013). Tectonic processes create fractures and faults, which can facilitate fluid flow and result in localized areas with high degrees of serpentinization. Mapping the extent of serpentinization at depth may yield information on the fluids' pathways. The combined modeling of gravity and magnetic data indicates that the vertical extent of the serpentinization is 400 m deep in the Storvannet valley (area 1, Figure 7a) and possibly 200 m deep in the plateau area (area 2, Figure 7a).

The model remains a simplified representation of the RUC. There are likely areas with varying amounts of alteration as observed in the drill core logs (Figure 3c) which cannot be resolved at our model scale. The least altered dunite rocks from the drill-core samples have a mean susceptibility and NRM value of 0.007 SI and 0.64 A/m respectively, and positive inclination. Site averages for NRM intensity of surface ultramafic rock samples range from 0.1 to 4.5 A/m, with one outlier NRM of 22 A/m that is a late-stage pyroxenite dike. NRM inclinations

Figure 7. Map view of the modeled serpentinized rocks with sensitivity tests along cross-section L5. (a) Contours of the thickness of the modeled serpentinized rocks superimposed on the aeromagnetic anomalies map. (b) Sensitivity tests along cross-section L5 show changes in the calculated magnetic anomaly using different NRM inclinations and Q ratios. Sensitivity tests illustrating changes of dip (c) and depth (d) of the entire deep UM part (light pink) illustrated on cross section L5. The differences between observed and calculated gravity and magnetic anomalies (residual anomalies) are shown above for each model. Black dots indicate gravity acquisition points with measurement error below 3 mGal. Black circled dots indicate gravity acquisition points with measurement error between 3 and 5 mGal.

vary between −37° and +84°. One notable feature of the serpentinized lithologies is that these samples have higher NRM intensities, carried by magnetite, with inclinations that are much shallower, or even negative. These directions clearly deviate from those of the more pristine rocks (Figure S3 in Supporting Information S1). In the Storvannet valley and in the central part of the CS these NRM directions are interpreted to cause the observed magnetic anomaly lows (below background).

In the Storvannet valley, assuming that the alteration is localized along the E-W fault, the thicknesses of the modeled altered rocks constrain the minimum depth extent of ultramafic rocks. In the plateau area, drill core logging and samples properties indicate that local serpentinization occurs in one major area in R3 and in two areas in R4 (Figure 3c). This alteration, if the remanent magnetization of the rock is reversely magnetized, could contribute to the reduced total magnetic field intensity. However, field and drill core logs observations suggest serpentinization in proximity of fault F3 occurs in steeply dipping veins of less than 1 m in thickness. Therefore, areas of serpentinization in the drill cores may represent narrow serpentinization zones. Given the lack of observation of extensive serpentinization in the field (excluding the Storvannet valley) and in the drill core samples, we consider the occurrence of magnetic sulfides as a possible source for a remanent magnetization of 12 A/m with a negative inclination on the plateau.

Previous electromagnetic studies (Thunehed, 2012) indicate in this area at approximately 100 m depth, the occurrence of layers enriched in sulfides with approximately 1 volume % of pyrrhotite. In R4 the sulfide-rich layers occur from 40 to 80 m below the surface in the Central Series dunite (Larsen et al., 2018, 2019). This is compatible with the local increase in susceptibility between 0.01 and 0.02 SI observed in the core log of R4 (black triangles on the R4 lithology-log in Figure 3c). The presence of magnetic pyrrhotite in the sulfide-rich layers could cause a local increase in magnetization. The NRM direction of the pyrrhotite would have been acquired later than the initial TRM of the RUC, due to its lower Curie temperature of 320°C. If the pyrrhotite is reversely magnetized, this could result in a magnetic low at this location. An alternative explanation could be a resetting of the magnetization during the Caledonian orogeny during a field reversal. According to Roberts (2007), this is the only known metamorphic event that affected the SIP after the emplacement.

6.2. Ore Mineralization

The RUC as well as the other ultramafic complexes in SIP formed during multiple magmatic recharge events along asthenosphere-lithosphere magmatic conduit systems partially facilitating a global LIP event. Large asthenosphere-rooted conduit systems are recognized as prime locations for the formation of so-called "World Class" Ni-Cu-PGE deposits (Maier and De Waal, 2001). Essentially, in conduit (or parasitic) magma-chambers, large Cu-Ni PGE deposits may form from the continuous supply of fertile magmas. A Ni-Cu and PGE deposit within the dunite has been proven by the deep drill cores (Grant et al., 2016; Larsen et al., 2018, 2019; Schanche et al., 2012). Modeling of a transient electromagnetic (TEM) survey describes this deposit as a continuous flat lying open bowl conductor at a depth of c. 40–100 m (Thunehed, 2012). Based on drill-core analysis a 40 m thick horizontal mineralized layer is present in this region. At a minimum depth of 40 m and a thickness of 40 m this mineralized layer is too small to measurably influence the gravity anomalies. A mineralized layer with a constant thickness of 40 m will cause a gravity anomaly of less than 3 mGal, which is below the resolution of our gravity data. Nevertheless, both gravity and magnetic methods succeeded in mapping lateral variations of the petrophysical properties of the ultramafic rocks at depth providing an important constraint on the distribution of the UM rocks at depth. According to Larsen et al. (2019) the most fertile mineralizations are associated with parasite chambers forming along the main conduit such as the example shown in the western part of profile L5 (Figure 7b). Therefore, our modeling succeeded in identifying a new parasitic side chamber, hence a potential target for exploration after Cu-Ni-Co-PGE mineralization.

Due to the inherent ambiguity of potential field interpretation, it is not possible to add further information to the geometry and lateral extension of the Ni-Cu-and the PGE deposit. However, we suggest that the magnetic anomaly low observed in the central part of the CS (Area 2, Figure 7a), and here modeled with the same parameters as the serpentinized zone in the Storvannet valley, could alternatively be due to the occurrence of pyrrhotite. Here, the resultant magnetization direction deviates both from the present-day geomagnetic field, and that found in the most pristine ultramafic rocks. In the most favorable case of

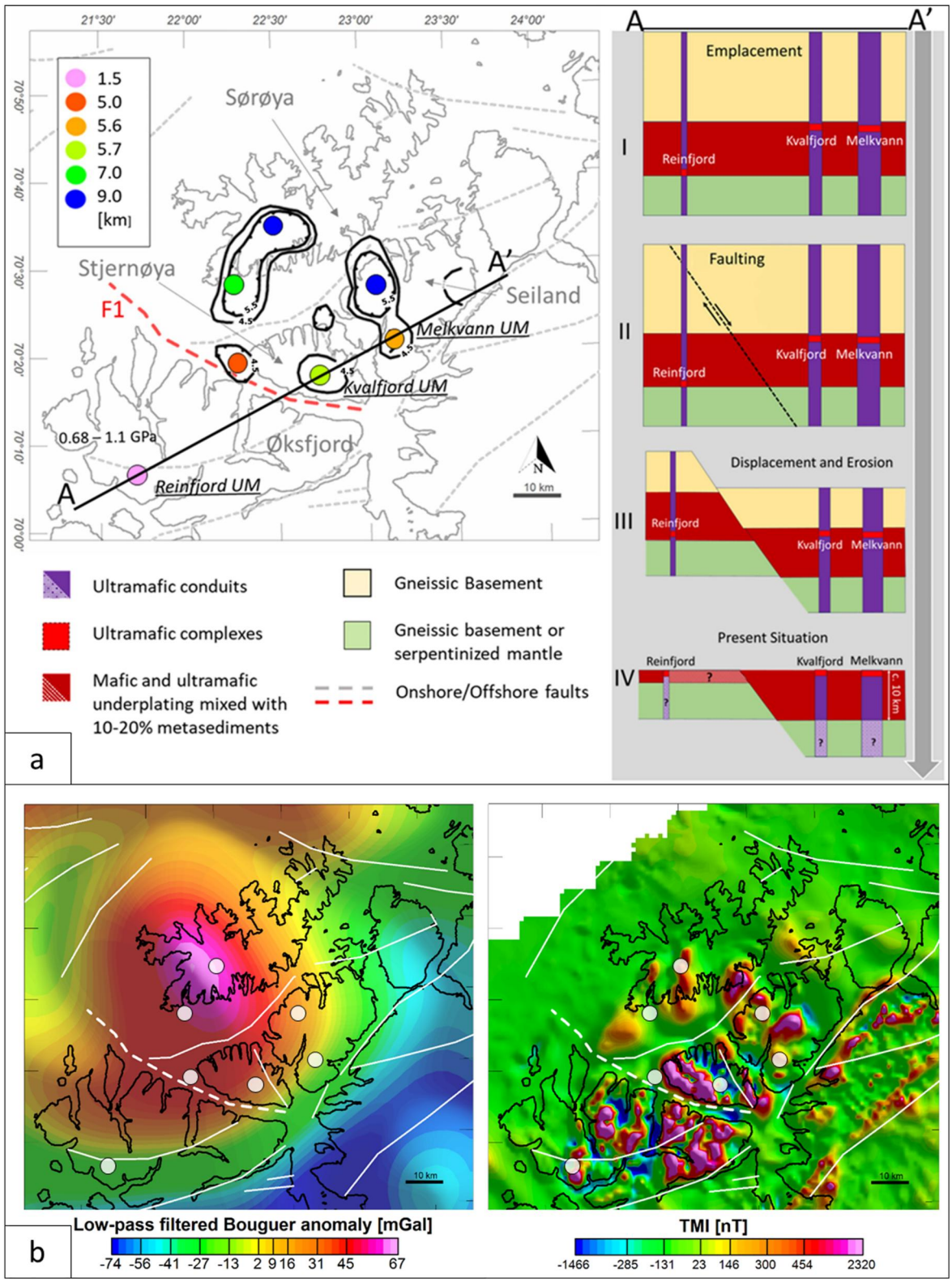

Figure 8.

magnetization direction opposite to the current inducing field, and assuming a susceptibility and a thickness for the mineralized layer of 0.02 SI and 40 m, respectively, to make a magnetic anomaly low of −500 nT, the rocks from this layer would need an NRM intensity of 12 A/m and a Q ratio >15 (Figure S4 in Supporting Information S1).

6.3. The RUC in the Tectonic Framework of the SIP

The RUC is the southernmost ultramafic complex of the SIP. Previous studies on the deep structure of the SIP from gravity modeling suggested that the province has several mafic/ultramafic mega-conduits arranged in an annular pattern (Pastore et al., 2016). Figure 8a shows that the deepest roots are below the islands of Seiland and Sørøya and reach a modeled depth of 9 km. Shallower roots with depth between 5 and 7 km are located below (a) the island of Stjernøya, (b) in the offshore area between the Øksfjord peninsula and the Sørøya island, and (c) below the southern part of the island of Seiland. The RUC is located more than 30 km south of this annular pattern. The modeled depth extent b.s.l. is approximately 1.4 km. This implies that the RUC has the shallowest of the ultramafic roots of the SIP or that the conduit forming the RUC is too narrow to produce a resolvable gravimetric and magnetic signature. Pastore et al. (2016) speculated whether the annular pattern of the roots north of the Oksfjord peninsula could indicate a major feeding system between the islands of Sørøya, Seiland and Stjernøya. The next question is the relation of this system with the RUC. Here, we consider a scenario where the RUC is not in the correct stratigraphic position with respect to the other ultramafic complexes, and that a different uplift event affected the crustal block hosting the RUC compared to the block hosting the other feeders north of the RUC. Based on petrological and geochemical evidence, Larsen et al. (2018), suggested that the RUC represents a deeper section compared to the northern ultramafic complexes in the SIP. The RUC also has a higher proportion of dunites exposed compared to the northern ultramafic complexes. At the same time, most of the exposed layered gabbros occur at the Øksfjord Peninsula. These observations can be described in a scenario where the gabbros and the ultramafic complexes of the Øksfjord Peninsula are underlain by lighter continental lithologies including the gneissic country rock. The modeling of the regional gravity data (Brooks, 1970; Olesen et al., 1990) provides the main evidence for selective uplift of the Øksfjord Peninsula with respect to the northern block of mafic-ultramafic intrusions (Figure 8a). A low-pass filtered Bouguer gravity anomaly map (Figure 8b) obtained using a cut-off wavelength of 40 km shows an elongated maximum in the NW-SE direction and a change in the gravity anomaly gradient from Stjernøya to the Øksfjord Peninsula. We suggest that this change could be explained by a normal fault complex uplifting the Øksfjord Peninsula by several kilometers (Figure 8). Recent studies by Koehl et al. (2019) support the occurrence of a major fault (F1 in Figure 8a) between the Øksfjord peninsula and the Stjernøya island based on comparison of satellite images with structural data, and aeromagnetic (Nasuti et al., 2015; Olesen et al., 2010) and bathymetry data. However, the magnetic anomaly pattern (Figure 8b) is quite complex to interpret due the inhomogeneous magnetic mineralogy across the SIP, and the drop in TMI in the area near the fault between Øksfjord and Stjernøya could be related to a small structural feature and not a high-displacement normal fault. Pressure estimates on the SIP rocks could support the need for substantial differential uplift. However, most of the available pressure estimates are based on contact metamorphic assemblages surrounding the ultramafic intrusions and are lower than the emplacement pressures recorded by the ultramafic assemblages. Future research on the emplacement temperatures and pressures of the different UM complexes (Kvalfjord, Melkvann, Nordre Brumandsfjord and Tappeluft) could reject or support these hypotheses. Because the underlying data comes with caveats, we cannot exclude an alternative hypothesis that the RUC is a secondary arm of the SIP magmatic conduit system, without later uplift of several kilometers with respect to the northern SIP ultramafic complexes.

Figure 8. (a) Regional map of the SIP with color-filled circles showing the approximate depth of the SIP at each locality with black contour lines highlighting the annular pattern of the roots (Pastore et al., 2016). Depths for the RUC (southern-most circle) were derived from this study. The root depths increase from southwest to northeast and a suggested explanatory evolution of the SIP in the sketch is shown to the right. Note that the fault complex (Koehl et al., 2019) is shown here in cross section as a unitary normal fault for simplicity. (b) Regional filtered Bouguer gravity (left) and magnetic data (right) (original data from the Geological survey of Norway, https://www.ngu.no/geologiske-kart) with main onshore/offshore faults from literature in white lines (the dashed line represents the master normal fault uplifting the Oksfjord Peninsula) and white filled circles for sites in (a) shown for comparison. Both gravity and magnetic anomaly maps shows a change in the area near the fault between Øksfjord and Stjernøya.

7. Conclusions

A new model of the buried architecture of the Reinfjord Ultramafic Complex (RUC) is derived from an extensive set of geophysical and petrophysical data and is summarized below:

- Modeling of the magnetic and the gravity anomalies supported by petrophysical properties suggests that the RUC is cylindrically shaped with a dunite core surrounded by wehrlite and gabbro. The modeled ultramafic part of the complex dips toward the NE and its maximum vertical extent is modeled to be approximately 1.4 km below sea level. The gabbro thickens toward east and toward north.
- The minimum estimated volume of RUC ultramafic rocks is 6.5 km^3. This is a small intrusive complex compared to other UM complexes of the SIP; however, it features a parasitic magma-chamber along a high yielding magmatic conduit system continuously supplying fertile melts that could be tapped for Cu, Ni, the PGE's and other metals.
- Magnetic methods refined the distribution of the rock types at, and below the surface, and identified areas of inhomogeneity among, and within, the different rock units. The distinct magnetic low in the Storvannet valley is interpreted to be caused by later serpentinization. Modeling and sensitivity tests indicate that rocks from this area have NRM values with shallow or negative inclinations, and high Q ratios.
- In the plateau area, southeast of the Storvannet valley, the magnetic survey maps an area of higher magnetic intensity. Here, an area with layers enriched in Cu and PGE has been suggested by earlier exploration surveys. The modeling of the magnetic anomaly supports the interpretation of a higher concentration of magnetic minerals, possibly pyrrhotite, in the uppermost 200 m of the Central Series.
- This new knowledge of the architecture of the RUC complex, viewed in the larger framework of the SIP intrusions, adds to the understanding of the geodynamic development of the SIP. The RUC is spatially separated from the other major UM complexes (Sørøya, Seiland and Stjernøya) which form the Northern part of the SIP. This model indicates that the RUC has a smaller depth extent than the other UM complexes. Combining these findings with constraints given by petrology, and known regional faults, we propose that the uplift history of the crustal block hosting the RUC differs from that in the northwestern part of the SIP. This interpretation which is supported by the regional gravity data would benefit from research focusing on the emplacement pressure and temperature conditions of the northern SIP ultramafic complexes.

Data Availability Statement

The land gravity and magnetic data files used in this paper to build the 3D model of the Reinfjord ultramafic complex and the model, are available at (Pastore et al., 2024) or upon request addressed to the corresponding author.

Acknowledgments
This work is dedicated to Oddmund Reinfjorden who provided logistical support during the fieldwork and in numerous other expeditions to Reinfjord with professionalism and friendliness, his enthusiasm will be greatly missed. The research was funded by the People Programme (Marie Curie Actions) of the European Union's Seventh Framework Programme FP7/2007-2013/ under REA-grant agreement No. 608001 "ABYSS," by the Research Council of Norway - NFR Grant 222666 to Prof. McEnroe and 324301 to Zeudia Pastore, we are grateful for the support from the NTNU department of Geoscience and Petroleum and Nordic Mining ASA, for and airborne geophysical data. The Platinum Probe project funded by the Nordic Council of Ministers to Prof. Larsen funded two of four drill cores. We greatly thank Richard Blakely, David Clark and an anonymous reviewer for their constructive comments and suggestions, and the Editor Mark Dekkers. We thank Thomas Grant, Kim Rune Grannes, Even Nikolaisen and Bjorn Eske Sørensen for field assistance. The Geological survey of Norway (NGU) provided LaCoste and Romberg G-569 gravimeter for use in fieldwork.

References

Bach, W., Paulick, H., Garrido, C. J., Ildefonse, B., Meurer, W. P., & Humphris, S. E. (2006). Unraveling the sequence of serpentinization reactions: Petrography, mineral chemistry, and petrophysics of serpentinites from MAR 15°N (ODP Leg 209, Site 1274). *Geophysical Research Letters*, *33*(13), L13306. https://doi.org/10.1029/2006GL025681

Bennett, M. C. (1974). The emplacement of a high temperature peridotite in the Seiland province of the Norwegian Caledonides. *Journal of the Geological Society*, *130*(3), 205–226. https://doi.org/10.1144/gsjgs.130.3.0205

Bennett, M. C., Emblin, S. R., Robins, B., & Yeo, W. J. A. (1986). High-temperature ultramafic complexes in the North Norwegian Caledonides: I–regional setting and field relationships. *Norges Geologiske Undersokelse Bulletin*, *405*, 1–40.

Blakely, R. J. (1996). *Potential theory in gravity and magnetic applications*. Cambridge University Press.

Brooks, M. (1970). A gravity survey of coastal areas of West Finnmark, Northern Norway. *Quarterly Journal of the Geological Society*, *125*(1–4), 171–192. https://doi.org/10.1144/gsjgs.125.1.0171

Clark, D. A. (1997). Magnetic petrophysics and magnetic petrology: Aids to geological interpretation of magnetic surveys. *AGSO Journal of Australian Geology and Geophysics*, *17*, 83–104.

Emblin, S. (1985). *The Reinfjord ultramafic complex, Seiland Province: Emplacement history and magma chamber model (Doctoral thesis)*. University of Bristol.

Evans, B., Hattori, K., & Baronnet, A. (2013). Serpentinite: What, why, where? *Elements*, *9*(2), 99–106. https://doi.org/10.2113/gselements.9.2.99

Finlay, C. C., Maus, S., Beggan, C. D., Bondar, T. N., Chambodut, A., Chernova, T. A., et al. (2010). International geomagnetic reference field: The eleventh generation. *Geophysical Journal International*, *183*(3), 1216–1230. https://doi.org/10.1111/j.1365-246X.2010.04804.x

Grannes, K. R. B. (2016). *Cryptic variations of olivene and clinopyroxene in the RF-4 drill-core: A geochemical study of the REINFJORD ultramafic complex, Norway (Master thesis)*. Norwegian University of Science and Technology.

Grant, T. B., Larsen, R. B., Anker-Rasch, L., Grannes, K. R., Iljina, M., McEnroe, S., et al. (2016). Anatomy of a deep crustal volcanic conduit system: The Reinfjord ultramafic complex, Seiland igneous province, northern Norway. *Lithos*, *252*, 200–215. https://doi.org/10.1016/j.lithos.2016.02.020

Grant, T. B., Larsen, R. B., Brown, E. L., Müller, A. B., & McEnroe, S. (2020). Mixing of heterogeneous, high-MgO, plume-derived magmas at the base of the crust in the Central Iapetus Magmatic Province (Ma 610-550): Origin of parental magmas to a global LIP event. *Lithos*, *364*, 105535. https://doi.org/10.1016/j.lithos.2020.105535

Griffin, W. L., Sturt, B. A., O'neill, C. J., Kirkland, C. L., & O'Reilly, S. Y. (2013). Intrusion and contamination of high-temperature dunitic magma: The Nordre Bumandsfjord pluton, Seiland, Arctic Norway. *Contributions to Mineralogy and Petrology*, *165*(5), 903–930. https://doi.org/10.1007/s00410-012-0841-6

Iljina, M. (2011a). Nickel, copper, platinum-group element, and gold potential of seiland igneous province, Norway. Report for Nordic Mining.

Iljina, M. (2011b). Exploration report on Reinfjord, Lokkarfjord and Tappeluft intrusions of the Seiland igneous province, Norway. In *In-house report for nordic mining*.

Johnson, D., & Asa, C. N. M. (2011). *Quality assessment and interpretation report on the Reinfjord and Lokkarfjord SkyTEM surveys*. Revelation Geoscience Ltd.

Koehl, J. B. K., Bergh, S. G., Osmundsen, P. T., Redfield, T. F., Indrevær, K., Lea, H., & Bergø, E. (2019). Late Devonian–Carboniferous faulting and controlling structures and fabrics in NW Finnmark. *Norwegian Journal of Geology*, *99*, 1–39. https://doi.org/10.17850/njg99-3-5

Larsen, R. B., Grant, T., Sørensen, B. E., Tegner, C., McEnroe, S., Pastore, Z., et al. (2018). Portrait of a giant deep-seated magmatic conduit system: The Seiland igneous province. *Lithos*, *296*, 600–622. https://doi.org/10.1016/j.lithos.2017.11.013

Larsen, R. B., Sørensen, B. E., & Nikolaisen, E. (2019). Formation and disruption of Cu-Ni-PGE deposits in a giant deep-seated mafic-ultramafic conduit system. In *Proceedings of the 15th Biennial SGA meeting* (pp. 27–30).

Maier, W. D., Li, C., & De Waal, S. A. (2001). Why are there no major Ni–Cu sulfide deposits in large layered mafic-ultramafic intrusions? *The Canadian Mineralogist*, *39*(2), 547–556. https://doi.org/10.2113/gscanmin.39.2.547

McCollom, T. M., & Seewald, J. S. (2013). Serpentinites, hydrogen, and life. *Elements*, *9*(2), 129–134. https://doi.org/10.2113/gselements.9.2.129

McEnroe, S. A., Brown, L. L., & Robinson, P. (2009a). Remanent and induced magnetic anomalies over a layered intrusion: Effects from crystal fractionation and magma recharge. *Tectonophysics*, *478*(1–2), 119–134. https://doi.org/10.1016/j.tecto.2008.11.021

McEnroe, S. A., Fabian, K., Robinson, P., Gaina, C., & Brown, L. L. (2009b). Crustal magnetism, lamellar magnetism and rocks that remember. *Elements*, *5*(4), 241–246. https://doi.org/10.2113/gselements.5.4.241

McEnroe, S. A., Harrison, R. J., Robinson, P., Golla, U., & Jercinovic, M. J. (2001). Effect of fine-scale microstructures in titanohematite on the acquisition and stability of natural remanent magnetization in granulite facies metamorphic rocks, southwest Sweden: Implications for crustal magnetism. *Journal of Geophysical Research*, *106*(B12), 30523–30546. https://doi.org/10.1029/2001JB000180

McEnroe, S. A., Robinson, P., Langenhorst, F., Frandsen, C., Terry, M. P., & Boffa Ballaran, T. (2007). Magnetization of exsolution intergrowths of hematite and ilmenite: Mineral chemistry, phase relations, and magnetic properties of hemo-ilmenite ores with micron-to nanometer-scale lamellae from Allard Lake, Quebec. *Journal of Geophysical Research*, *112*(B10), B10103. https://doi.org/10.1029/2007JB004973

Michels, A., McEnroe, S., & Fichler, C. (2018). Geophysical expression of the Leka Ophiolite, Norway modeled from integrated gravity, magnetic and petrophysical data. *Norsk Geologisk Tidsskrift*, *98*(1), 103–125. https://doi.org/10.17850/njg98-1-07

Miller, D. J., & Christensen, N. I. (1997). Seismic velocities of lower crustal and upper mantle rocks from the slow-spreading Mid-Atlantic Ridge, south of the Kane Transform Zone (MARK). *Proceedings of the Ocean Drilling Program Scientific Results*, *153*, 153. https://doi.org/10.2973/odp.proc.sr.153.043.1997

Nasuti, A., Roberts, D., Dumais, M.-A., Ofstad, F., Hyvönen, E., Stampolidis, A., & Rodionov, A. (2015). New high-resolution aeromagnetic and radiometric surveys in Finnmark and north Troms: Linking anomaly patterns to bedrock geology and structure. *Norwegian Journal of Geology*, *95*, 217–243. https://doi.org/10.17850/njg95-3-10

Oldenburg, D. W., & Pratt, D. A. (2007). Geophysical inversion for mineral exploration: A decade of progress in theory and practice. *Proceedings of Exploration*, *7*(5), 61–95.

Olesen, O., Ebbing, J., Gellein, J., Gernigon, L., Koziel, J., Lauritsen, T., et al. (2010). New aeromagnetic and gravity compilations from Norway and adjacent areas – Methods and applications. In B. A. Vining & S. C. Pickering (Eds.), *Petroleum geology: From mature basins to new frontiers* (pp. 559–586). Geological Society of London.

Olesen, O., Roberts, D., Henkel, H., Lile, O. B., & Torsvik, T. H. (1990). Aeromagnetic and gravimetric interpretation of regional structural features in the Caledonides of west Finnmark and north Troms, northern Norway. Norges Geologiske Undersøkelse. *Bulletin*, *419*, 1–24.

Orvik, A. S., Sørensen, B. E., Larsen, R. B., & Slagstad, T. (2019). The dike swarm in the Reinfjord ultramafic complex: A window in to the terminal stages forming the Seiland igneous province, N. Norway. In *Abstracts and proceedings, of the geological society of Norway, 33rd geological winter meeting*.

Oufi, O., Cannat, M., & Horen, H. (2002). Magnetic properties of variably serpentinized abyssal peridotites. *Journal of Geophysical Research*, *107*(B5), EPM-3. https://doi.org/10.1029/2001JB000549

Pastore, Z., Church, N. S., Fichler, C., Michels, A., ter Maat, G., Larsen, R. B., & McEnroe, S. A. (2024). Replication data for "the architecture of a root zone of a large magmatic conduit system from high resolution magnetic, gravity and petrophysical data: The Reinfjord ultramafic complex"" (version 1) [Dataset]. *DataverseNO*. https://doi.org/10.18710/QXQBKG

Pastore, Z., Fichler, C., & McEnroe, S. A. (2016). The deep crustal structure of the mafic–ultramafic Seiland Igneous Province of Norway from 3-D gravity modeling and geological implications. *Geophysical Journal International*, *207*(3), 1653–1666. https://doi.org/10.1093/gji/ggw362

Pastore, Z., McEnroe, S. A., ter Maat, G. W., Oda, H., Church, N. S., & Fumagalli, P. (2018). Mapping magnetic sources at the millimeter to micrometer scale in dunite and serpentinite by high-resolution magnetic microscopy. *Lithos*, *323*, 174–190. https://doi.org/10.1016/j.lithos.2018.09.018

Pratt, D. A., Foss, C. A., & Roberts, S. (2006). User guided inversion & visualisation of interpretation confidence. In *Paper presented at AESC conference, Melbourne: extended abstract. Australian Earth sciences convention (AESC)*. Retrieved from http://www.tensor-research.com.au/home/further-reading

Roberts, R. J. (2007). *The seiland igneous province, northern Norway: Age, provenance, and tectonic significance (Doctoral dissertation)*. University of the Witwatersrand.

Roberts, R. J., Corfu, F., Torsvik, T. H., Hetherington, C. J., & Ashwal, L. D. (2010). Age of alkaline rocks in the Seiland igneous province, northern Norway. *Journal of the Geological Society*, *167*(1), 71–81. https://doi.org/10.1144/0016-76492009-014

Robinson, P., McEnroe, S. A., Miyajima, N., Fabian, K., & Church, N. (2016). Remanent magnetization, magnetic coupling, and interface ionic configurations of intergrown rhombohedral and cubic Fe-Ti oxides: A short survey. *American Mineralogist*, *101*(3), 518–530. https://doi.org/10.2138/am-2016-5519

Ryan, E. J., Sørensen, B. E., Drivenes, K., & Larsen, R. B. (2022). Infiltration of volatile-rich mafic melt in lower crustal peridotites provokes lower crustal earthquakes. *Journal of Structural Geology*, *163*, 104708. https://doi.org/10.1016/j.jsg.2022.104708

Schanche, M., Iljina, M., & Larsen, R. (2012). New nickel, copper and platinum-group element discoveries in northern Norway. *Mineralproduksj*, *2*, 91–99.

SkyTEM Surveys. (2011). SkyTEM survey: Lokkarfjord and Reinfjord, Finmark county, Norway, data report: Technical report prepared for Nordic mining ASA, September 2011. Retrieved from http://www.nordicmining.com/new-nickel-copper-and-platinum-group-element-discoveries-in-north-norway

Sørensen, B. E., Grant, T., Ryan, E. J., & Larsen, R. B. (2019). In situ evidence of earthquakes near the crust mantle boundary initiated by mantle CO_2 fluxing and reaction-driven strain softening. *Earth and Planetary Science Letters*, *524*, 115713. https://doi.org/10.1016/j.epsl.2019.115713

ter Maat, G. W., Church, N. S., Oda, H., Pastore, Z., & McEnroe, S. A. (2024). Characterization and imaging magnetic minerals from ultramafic roots of a LIP: Implication for deep crustal magnetic sources. *Geophysical Journal International*, *236*(3), 1577–1595. https://doi.org/10.1093/gji/ggad479

ter Maat, G. W., McEnroe, S. A., Church, N. S., & Larsen, R. B. (2019). Magnetic mineralogy and petrophysical properties of ultramafic rocks: Consequences for crustal magnetism. *Geochemistry, Geophysics, Geosystems*, *20*(4), 1794–1817. https://doi.org/10.1029/2018GC008132

Thunehed, H. (2012). *TEM-survey at Reinfjord–survey and interpretation report*. Geovista AB: Luleå, Sweeden.

References From the Supporting Information

Hoffmann-Rothe, A., Ritter, O., & Janssen, C. (2004). Correlation of electrical conductivity and structural damage at a major strike-slip fault in northern Chile. *Journal of Geophysical Research*, *109*(B10), B10101. https://doi.org/10.1029/2004JB003030